

The First DIRECT Distance Determination to a Detached Eclipsing Binary in M33¹

A. Z. Bonanos², K. Z. Stanek³, R. P. Kudritzki⁴, L.M. Macri^{5,6}, D. D. Sasselov⁷,
 J. Kaluzny⁸, P. B. Stetson⁹, D. Bersier¹⁰, F. Bresolin⁴, T. Matheson⁵,
 B.J. Mochejska⁸, N. Przybilla^{4,11}, A.H. Szentgyorgyi⁷, J. Tonry⁴, G. Torres⁷

ABSTRACT

We present the first direct distance determination to a detached eclipsing binary in M33, which was found by the DIRECT Project. Located in the OB 66 association at coordinates $(\alpha, \delta) = (01:33:46.17, +30:44:39.9)$ for J2000.0, it was one of the most suitable detached eclipsing binaries found by DIRECT for distance determination, given its apparent magnitude and orbital period. We obtained follow-up *BV* time series photometry, *JHK_s* photometry and optical

¹Based on observations obtained with 1.2 meter FLWO, 2.1 meter KPNO, 3.5 meter WIYN, 8.2 meter Gemini, and 10 meter Keck-2 telescopes.

²Vera Rubin Fellow, Carnegie Institution of Washington, Department of Terrestrial Magnetism, 5241 Broad Branch Road NW, Washington, DC 20015; bonanos@dtm.ciw.edu

³Department of Astronomy, The Ohio State University, 140 W. 18th Avenue, Columbus, OH 43210; kstanek@astronomy.ohio-state.edu

⁴Institute for Astronomy, University of Hawaii, 2680 Woodlawn Drive, Honolulu, HI 96822; kud, bresolin, jt@ifa.hawaii.edu.

⁵National Optical Astronomy Observatory, 950 North Cherry Avenue, Tucson, AZ 85719; lmacri, matheson@noao.edu.

⁶Hubble Fellow & Goldberg Fellow.

⁷Harvard-Smithsonian Center for Astrophysics, 60 Garden St., Cambridge, MA 02138; sasselov, aszentgyorgyi, torres@cfa.harvard.edu.

⁸Copernicus Astronomical Center, Bartycka 18, 00-716 Warszawa, Poland; jka, mochejsk@camk.edu.pl.

⁹National Research Council of Canada, Herzberg Institute of Astrophysics, 5071 West Saanich Road, Victoria, BC V9E 2E7, Canada; peter.stetson@nrc-cnrc.gc.ca

¹⁰Liverpool John Moores University, Twelve Quays House, Egerton Wharf, Birkenhead, CH41 1LD, United Kingdom; dbf@astro.livjm.ac.uk.

¹¹Dr. Remeis-Sternwarte, Astronomical Institute of the University of Erlangen-Nuremberg, Sternwartstrasse 7, D-96049 Bamberg, Germany; przybilla@sternwarte.uni-erlangen.de.

spectroscopy from which we determined the parameters of the system. It contains two O7 main sequence stars with masses of $33.4 \pm 3.5 M_{\odot}$ and $30.0 \pm 3.3 M_{\odot}$ and radii of $12.3 \pm 0.4 R_{\odot}$ and $8.8 \pm 0.3 R_{\odot}$, respectively. We derive temperatures of 37000 ± 1500 K and 35600 ± 1500 K. Using $BVRJHK_s$ photometry for the flux calibration, we obtain a distance modulus of 24.92 ± 0.12 mag (964 ± 54 kpc), which is ~ 0.3 mag longer than the Key Project distance to M33. We discuss the implications of our result and the importance of establishing M33 as an independent rung on the cosmological distance ladder.

Subject headings: binaries: eclipsing – binaries: spectroscopic – distance scale – stars: fundamental parameters- galaxies: individual (M33)

1. Introduction

Starting in 1996 we undertook a long term project, DIRECT (i.e. “direct distances”), to obtain the distances to two important galaxies in the cosmological distance ladder, M31 and M33. These “direct” distances are obtained by measuring the absolute distance to detached eclipsing binaries (DEBs).

M31 and M33 are the nearest and most suitable Local Group galaxies for calibrating the extragalactic distance scale. However, they present a much greater observational challenge than the current anchor of the distance scale, the Large Magellanic Cloud (LMC). Their greater distance makes the brightest stars in them appear ~ 6 mag fainter than the brightest LMC stars, thus pushing the limit of current spectroscopic capabilities. In addition, crowding and blending become more significant with increasing distance (Mochejska et al. 2000, 2001c). Unfortunately, distances are now known to no better than 10-15%, as there are discrepancies of 0.2 – 0.3 mag between various distance indicators (e.g. Benedict et al. 2002, Figure 8). These uncertainties limit the calibration of stellar luminosities and population synthesis models for early galaxy formation and evolution.

DEBs have the potential to establish distances to M31 and M33 with an unprecedented accuracy of 5% (for reviews and history of method see Andersen 1991; Hilditch 1996; Paczynski 1997; Kruszewski & Semeniuk 1999). They offer a single step distance determination to nearby galaxies and may therefore provide an accurate zero point calibration of various distance indicators – a major step towards very accurate and independent determination of the Hubble constant. In the last few years, eclipsing binaries have been used to obtain accurate distance estimates to the Large Magellanic Cloud (e.g. Guinan et al. 1998; Fitzpatrick et al. 2003), the Small Magellanic Cloud (Harries et al. 2003; Hilditch et al. 2005) and most

recently to a semi-detached system in M31 (Ribas et al. 2005). Distances to individual eclipsing binaries in the Magellanic Clouds are claimed to be accurate to better than 5%.

Detached eclipsing binaries have yet to be used as distance indicators to M31 and M33. The DIRECT project has initiated a search for DEBs and new Cepheids in the M31 and M33 galaxies. We have analyzed five $11' \times 11'$ fields in M31, A-D and F (Kaluzny et al. 1998; Stanek et al. 1998, 1999; Kaluzny et al. 1999; Mochejska et al. 1999, hereafter Papers I, II, III, IV, V) and one $22' \times 22'$ field, Y (Bonanos et al. 2003, hereafter Paper IX). A total of 674 variables, mostly new, were found: 89 eclipsing binaries, 332 Cepheids and 253 other periodic, possible long-period or non-periodic variables. We have analyzed two fields in M33, A and B (Macri et al. 2001, hereafter Paper VI) and found 544 variables: 47 eclipsing binaries, 251 Cepheids and 246 other variables. Follow up observations of fields M33A and M33B produced 280 and 612 new variables, respectively (Mochejska et al. 2001a,b, hereafter Papers VII, VIII), including 101 new eclipsing binaries. Variables from two more DIRECT fields, one in M31 and the other in M33, remain to be reported.

Of the 237 eclipsing binaries found by DIRECT, only four are bright enough ($V_{max} < 20$ mag) for distance determination with currently available telescopes. An additional criterion for selection is that they contain deep eclipses, which removes degeneracies in the modeling. D33J013346.2+304439.9 is the brightest of these, discovered in field M33A (Paper VI), and this paper presents the distance we obtained to it with subsequent observations. In §2 we describe the observations and the data reduction, in §3 we present the light curve and radial velocity curve analysis, in §4 the distance determination and in §5 the discussion.

2. Observations

The DIRECT Project discovered the detached eclipsing binary D33J013346.2+304439.9 ($\alpha = 01:33:46.17$, $\delta = +30:44:39.9$: J2000.0) in field M33A (Paper VI), using the F.L. Whipple Observatory 1.2 meter telescope between 1996 September and 1997 October.

2.1. Follow-up V and B -band Photometry

In 1999 and 2001 we obtained follow-up photometry with the Tektronix 2048×2048 CCD (T2KA camera) at the KPNO 2.1 m telescope, with a pixel scale of $0''.305 \text{ pixel}^{-1}$. The 1999 observations are described in Paper VII. We additionally obtained $94 \times 600s$ exposures in the V -band and $19 \times 600s$ in B -band in October 2001. Tables 1 and 2 present the BV

light curves. The images were processed with standard IRAF¹ routines. The nonlinearity of the CCD was corrected with the method outlined in Paper VII.

The photometry for the variable stars was extracted using the ISIS image subtraction package (Alard & Lupton 1998; Alard 2000) from the V and B -band data. We followed the ISIS reduction procedure described in detail in Paper VII. DAOPHOT/ALLSTAR PSF photometry was performed on the B and V reference image separately and aperture corrections were applied before converting the flux light curves to instrumental magnitudes. In addition, we performed DAOPHOT PSF photometry on all frames to verify that the shapes of the light curves were correctly measured with ISIS.

Observations of the DEB were also obtained with the MiniMosaic CCD camera on the WIYN² 3.5 meter telescope at KPNO, with a pixel scale of $0''.28 \text{ pixel}^{-1}$. On 1999 October 3, we obtained a 300s exposure in each of the V and B -bands at airmass 1.28 and 1.25, respectively and at phase 0.73. Conditions were photometric, and 3 Landolt standard fields were observed, covering a range in airmass from 1.17 to 1.40. These data were used for calibrating the BV light curves to standard photometric bands (Landolt 1992).

2.2. Photometric Calibration

The aperture photometry of the stars in the Landolt (1992) fields was derived with DAOGROW (Stetson 1990). The photometric solutions were very robust (rms ~ 0.03 mag). Instrumental magnitudes were derived with DAOPHOT/ALLSTAR and aperture corrections with DAOGROW after subtraction of all but PSF stars. As for standards the largest aperture was set to 24 pixels. The WIYN calibration yielded $V = 19.51 \pm 0.01$ mag, $B - V = -0.20 \pm 0.01$ mag for the DEB.

Other surveys of M33 have measured photometry for the DEB: Massey et al. (1996, Star UIT196) and Ivanov et al. (1993, Star 929), however the quality of the data is inferior. The Local Group Survey (Massey et al. 2006) has obtained high quality photometry of the DEB, using the KPNO 4-meter telescope. They measured out of eclipse magnitudes of $V = 19.52 \pm 0.01$, $B - V = -0.20 \pm 0.01$, $U - B = -1.14 \pm 0.01$, $V - R = -0.12 \pm 0.01$, $R - I = -0.18 \pm 0.01$, in excellent agreement with our BV values. Henceforth, we use the

¹IRAF is distributed by the National Optical Astronomy Observatory, which are operated by the Association of Universities for Research in Astronomy, Inc., under cooperative agreement with the NSF.

²The WIYN Observatory is a joint facility of the University of Wisconsin-Madison, Indiana University, Yale University, and the National Optical Astronomy Observatory.

average of these values: $B = 19.32 \pm 0.01$ and $V = 19.52 \pm 0.01$.

2.3. Near-Infrared Photometry

We carried out near-infrared observations of the DEB using the Gemini North telescope and NIRI (Hodapp et al. 2003) as queue program GN-2005B-DD-4. We observed the system in the J , H and K_s bandpasses on 2006 January 03 (UT) between phases 0.39 – 0.40. Conditions were photometric and the range of airmasses was between 1.05 and 1.25. The typical PSF FWHM was $0''.3$, or 2.5 pix at the $f/6$ plate scale of NIRI. Total on-source exposure times were 11 minutes in J , 35 minutes in H , and 32 minutes in K_s , with individual exposures of 30s in J and H and 60s in K_s .

We reduced the images (bad pixel masking, dark current correction, sky subtraction and flat fielding) using the IRAF Gemini NIRI package (v1.8). We performed PSF photometry using DAOPHOT and ALLSTAR (Stetson 1987) on each individual image, because the PSF exhibited significant variations in ellipticity from image to image. We defined the PSF out to a radius of 8 pixels ($0''.94$) which included essentially all of the stellar flux. Aperture corrections were derived using DAOGROW (Stetson 1990) and amounted to $\lesssim 0.02$ mag.

We calibrated the photometry using several 2MASS stars in the field of view that were determined to be isolated from our higher-resolution Gemini images. In some cases, we added the flux of faint neighboring stars to that of the bright comparison star, since they appear unresolved in the 2MASS images. We determined effective zeropoints for this Gemini/NIRI dataset (at airmass ~ 1.1 and $J - K_s \sim 1$) of 23.82, 23.75, and 23.23 ± 0.05 mag for J , H and K_s , respectively (corresponding to the 2MASS magnitude of a star that would yield 1 ADU/sec). By following this calibration path, we found mean out-of-eclipse magnitudes for the DEB of $J = 20.02 \pm 0.05$, $H = 20.05 \pm 0.06$ and $K_s = 20.13 \pm 0.06$ mag.

Figure 1 is a K_s -band finder chart of the field, indicating the location of the DEB and the photometric calibration reference stars in both the Gemini/NIRI and 2MASS images.

2.4. Spectroscopic Observations

We obtained spectra of the DEB over 7 epochs, 6 half and 1 full night (2004 Oct 11 UT), in the fall of 2002, 2003 and 2004 with the Echellette Spectrograph and Imager (or ESI, Sheinis et al. 2002) on the 10-meter Keck-II telescope on Mauna Kea. In the fall of 2004, we also obtained 4 sets of 5×2700 s spectra at quadrature with the B1200 lines/mm grating of the Gemini Multi Object Spectrograph (GMOS, Hook et al. 2003) on the Gemini-North

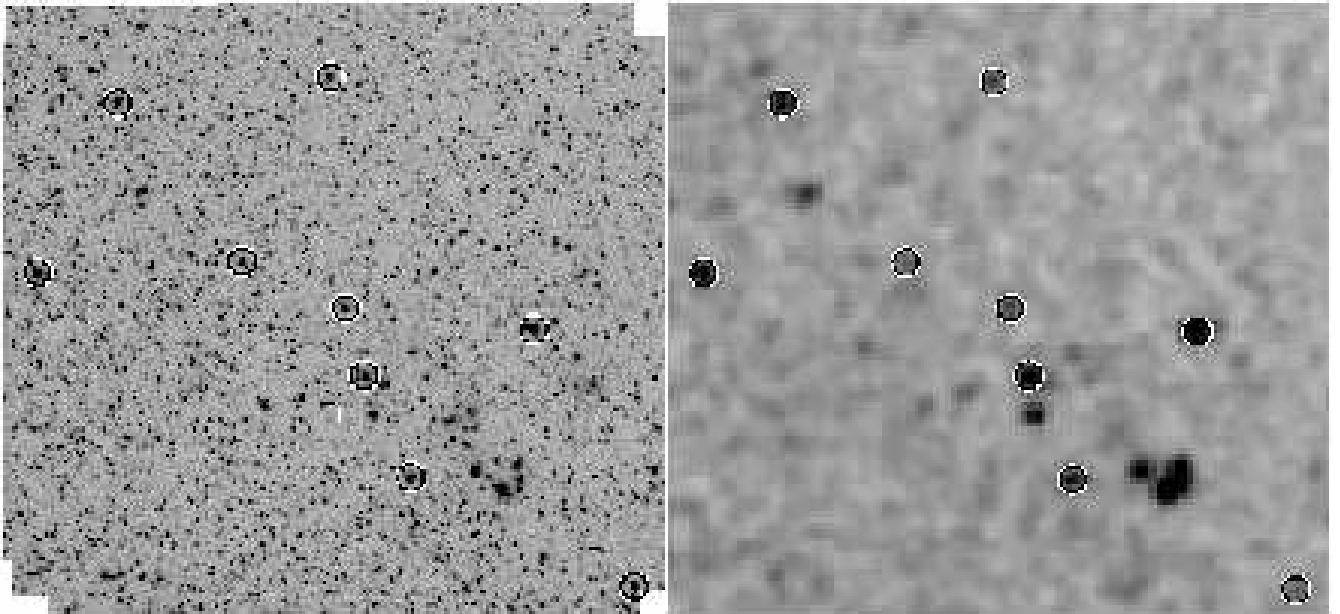


Fig. 1.— K_s -band finder chart, $1''.8 \times 1''.8$, N is up, E to the left. The circles indicate the stars used for calibration on both the NIRC2 image (Left) and the 2MASS image (Right). The DEB is marked on the NIRC2 image by the crosshairs.

8-meter telescope on Mauna Kea. Table 3 summarizes the exposure times and dates of observations, which total 4 nights on Keck and 19 hours on Gemini. The ESI spectra range from $3950 - 10000\text{\AA}$, have a reciprocal dispersion of $11 \text{ km s}^{-1}/\text{pix}$ and with a $1''$ slit we achieved a velocity resolution of 74 km s^{-1} . The GMOS spectra range from $3770 - 5227\text{\AA}$, have a $0.23 \text{ \AA}/\text{pix}$ dispersion and with a $0''.75$ slit we achieved a resolution of 120 km s^{-1} . The signal to noise (S/N) of the spectra ranges from 15-40. Observations were taken at low airmass and the slit was rotated 75 deg East from the North to minimize contamination from nearby H II regions.

Standard CCD processing was done with IRAF. We used the algorithm of Pych (2004) for cosmic ray rejection from each two dimensional image. We then optimally extracted the spectra and calibrated them in wavelength with IRAF routines. Three copper-argon calibration spectra were interspersed between the 5 sets of GMOS spectra. In 2002, we found ESI to be stable to a fraction of a pixel, thus in subsequent runs we only took several CuAr and HgNeXe lamps at the beginning and end of the night (or half night) that we averaged together and used to establish the wavelength solution, with low-order polynomial fits to the lamps. The small spatial extent of the ESI slit made background subtraction difficult at the Balmer lines. Such contamination does not affect the lines used for radial velocity determination, however. Spectra of standard stars were obtained at each epoch with

ESI and were used to calibrate the DEB in flux and to remove telluric lines with our IDL routines (Wade & Horne 1988; Matheson et al. 2000).

We used the IRAF Gemini package v1.7 to reduce the GMOS data. We wavelength calibrated the 3 extensions/chips of each exposure separately with copper-argon lamps for a more accurate wavelength calibration and merged the extensions at the end. The gaps between chips correspond to the regions $4244 - 4255 \text{ \AA}$ and $4731 - 4747 \text{ \AA}$ in the spectrum. For the flux calibration we used standard star spectra that were observed nearest in time to the DEB. The observations from each night were averaged together, weighting by the exposure times. Finally, we normalized the combined spectra, dividing them by a spline function which we fit interactively to points in the continuum region.

Absorption lines from both stars are clearly resolved in the spectrum. We were not able to avoid emission from nearby H II regions, thus our spectra contain strong nebular emission in the hydrogen lines and weaker emission in some of the helium lines, as well as forbidden oxygen lines [O III] $\lambda\lambda 4959, 5007$. The GMOS spectra show broad Ca II $\lambda 3933.7$ absorption and a narrow absorption line at $\lambda 4433.3$, possibly due to an interstellar band.

3. Light Curve and Radial Velocity Curve Analysis

Initially, we used the multiharmonic analysis of variance technique (Schwarzenberg-Czerny 1989, 1996) to search the light curves for periodicity. We merged the B and V light curves, scaled to V , and searched for the best period by fitting a Gaussian to the peak of the periodogram generated by this method and found a period $P = 4.8935$ days, which serves as the initial guess for the modeling. In this paper, we define the primary star (star 1) photometrically, as the hotter star producing the deeper eclipse at phase zero. In the analysis below, we show the primary to be the larger and more massive star also.

3.1. Initial Light Curve Parameter Estimation

We first estimated the parameters of the V -band light curve with the EBOP code (Nelson & Davis 1972; Popper & Etzel 1981). We computed fits for several periods and found the fit with a period of $P = 4.8938$ days to have the smallest residuals. Bootstrap analysis (Press et al. 1992) yielded very small values for the errors, $\sim 2\%$, which are smaller than errors from the radial velocity curves discussed later on.

EBOP’s biaxial ellipsoidal approximation holds for values of oblateness ϵ less than 0.04 and fractional radii less than 0.2. We find $\epsilon = 0.02$, but a fractional radius for the primary

slightly larger than 0.2, thus we proceed to a more detailed treatment. Using the EBOP parameters as starting values, we fit the 83 B -band points and the 278 V -band points in the light curve simultaneously with the April 2003 version of the Wilson-Devinney (WD) program (Wilson & Devinney 1971; Wilson 1979, 1990; van Hamme & Wilson 2003) in the detached mode (MODE=2). We found the following best fit parameters: eccentricity $e = 0.17$, $\omega = 251.8$ deg, inclination $i = 86.9$ deg, light ratio $L_2/L_1 = 0.4912$ in V and 0.4923 in B and flux ratio $F_1/F_2 = 1.039$ in V and 1.036 in B , in agreement with the definition of the primary being the hotter star. These preliminary values were refined later (see §3.3) in a simultaneous fit of both light curves and radial velocity curves. In eccentric binaries, there is a degeneracy in determining the radius and luminosity ratio from the light curves alone. We found that reversing the radii so that the primary is smaller and less luminous also produced a good light curve fit. We resolve this by using the spectroscopic light ratio in §3.4.

3.2. TODCOR Analysis of Spectra

We used the method of two dimensional cross correlation or TODCOR, developed by Zucker & Mazeh (1994), to measure radial velocities of the stars in the DEB. TODCOR can distinguish small velocity separations even more accurately than one dimensional cross correlation. Initially, we calculated a grid of template spectra over a range of temperatures around 30000 K using the LTE ATLAS9 models and opacities developed by Kurucz (1993). We ran TODCOR with ATLAS9 template spectra and found preliminary values for the semi-amplitudes, mass ratio and thus the semi-major axis. We thus obtained estimates for $\log(g)$ and the masses from which we computed a grid of non-local thermodynamic equilibrium (NLTE) spectra with FASTWIND (Santolaya-Rey et al. 1997; Puls et al. 2005). This hydrodynamic NLTE code includes stellar winds, spherical extension and metal line blanketing of millions of lines in (approximate) NLTE. We found the best fit spectra to have effective temperatures $T_{\text{eff1}} = 37000 \pm 1500$ K and $T_{\text{eff2}} = 35600 \pm 1500$ K. A detailed description of the temperature determination follows in §3.4.

The NLTE spectra were used to derive the final radial velocities of the stars. We prepared them for TODCOR by applying rotational broadening of 120 km s^{-1} which was determined from the spectral fits. We also applied instrumental broadening to match the resolution of the observations, by convolving the models with a Gaussian of appropriate FWHM for ESI and GMOS. The IRAF *rvsao.xcsao* (Tonry & Davis 1979; Kurtz et al. 1992) task was used to compute the one dimensional cross correlation function, required by TODCOR, for each observed spectrum with the appropriate model. We used the range

3975 – 6000 Å for ESI spectra and 3950 – 5227 Å for GMOS spectra, excluding the Balmer lines and [O III] emission lines. We ran TODCOR with model spectra containing only hydrogen and helium lines, masking out the broad hydrogen lines, and assuming a luminosity ratio $L_2/L_1 = 0.49$ found from the light curve analysis. Table 4 presents the measured velocities for each spectrum. The spectrum of 20021101 at phase 0.595 produced a spurious velocity for the secondary star. We excluded it from further analysis because this spectrum has the lowest S/N (~ 15) and the secondary contributes only half the amount of light to the spectrum which makes it even harder to measure. The velocities measured are robust and accurate to 30 km s^{-1} . As a final test we ran TODCOR using ATLAS9 models (37000K, 36000K with $\log(g) = 4$) and TLUSTY (Lanz & Hubeny 2003) models including metals (37500K for both stars and $\log(g) = 3.75$ and 4.00). Both runs produced radial velocities and semi-amplitudes in agreement within errors.

From the radial velocity curve analysis alone, we found a mass ratio $q = M_2/M_1 = 0.90 \pm 0.06$, velocity semi-amplitudes of $K_1 = 240 \pm 11 \text{ km s}^{-1}$ and $K_2 = 268 \pm 11 \text{ km s}^{-1}$, systemic velocity $\gamma = -214.1 \pm 6.8 \text{ km s}^{-1}$ and semi-major axis $a \sin i = 48.3 \pm 1.6 R_\odot$ and minimum masses of $M_1 \sin^3 i = 33.3 \pm 3.5 M_\odot$ and $M_2 \sin^3 i = 29.9 \pm 3.3 M_\odot$, fixing e and ω from the preliminary light curve analysis described above.

Measuring radial velocities of early-type stars is complex for several reasons: they have very few lines and the strongest of these, mainly the Balmer lines, are broadened due to rotation and the Stark effect. The standard one dimensional cross correlation method has been shown to produce systematically smaller semi-amplitudes when blended lines are included. Hilditch (2001) estimates the effect to be $\sim 50\%$ for hydrogen lines and $\sim 10\%$ for helium lines, for velocity differences between components of less than 200 km s^{-1} . However, with TODCOR systematic errors due to blending are avoided. Finally, the rotational velocity used in the synthetic spectrum is also a source of systematic error, if it deviates from the true value. The value of $v \sin i$ fit to the spectra is accurate to $\sim 20 \text{ km s}^{-1}$.

We attempted to use the spectral disentangling technique (Simon & Sturm 1994) which has been shown to be superior to standard one dimensional cross correlation by Harmanec et al. (1997) in yielding more accurate velocities. We used the public code FDBinary (Ilijic et al. 2001, 2004), but found significantly different semi-amplitudes than those from the TODCOR analysis with unrealistically small errors and concluded that higher signal to noise spectra ($S/N \geq 40$) at all epochs are required for this method to give meaningful results. The presence of nebular emission lines, even though masked out, may also have hindered this method.

3.3. Combined Analysis of LC and RV curves

With the radial velocity measurements in hand, we proceeded to perform a simultaneous fit of the BV light curves and the radial velocity curves with WD in the detached mode (MODE 2) for 13 parameters: the inclination i , eccentricity e , the argument of periastron ω_0 , the semi-major axis a , system center of mass radial velocity γ , the surface potential for each star Ω_1 and Ω_2 , mass ratio $q = M_2/M_1$, $T_{\text{eff}2}$, period P , time of primary eclipse T_0 , and band pass luminosity L_1 in each band.

Following the advice of van Hamme (1993), we used the square root limb darkening law which gives better results for hot stars in the optical. Theoretical bolometric and passband specific limb darkening coefficients were taken from theoretical values from Claret (2000) for a LTE ATLAS9 stellar atmosphere model with $T_{\text{eff}} = 37000$ K, $\log(g) = 4.0$ (cgs), turbulent velocity of 4 km s^{-1} and solar metallicity. We fixed gravity brightening exponents to unity and albedos to 0.5 from theoretical values (Hilditch 2001) for stars at such temperatures. For reflection, we used a MREF value of 1 for simple treatment of reflection with the inverse square law. Additionally, we allowed for non Keplerian effects on the radial velocity curve. All data points were weighted equally.

We defined convergence to be reached after three consecutive iterations for which the corrections for all adjusted parameters were smaller than their respective standard or statistical errors (e.g., Kallrath & Milone 1999). The results of the fit and 1σ errors are given in Table 5 and the derived physical parameters in Table 6. The rms residuals were 0.01 for both B and V light curves. Figures 2 and 3 show the V and B -band light curve model fits for the DEB. Note that the deviation of the secondary eclipse from phase 0.5 is due to the eccentricity of the system. The radial velocity curve is presented in Figure 4. The rms residuals are 26.0 km s^{-1} for the primary and 28.0 km s^{-1} for the secondary star. The ephemeris is:

$$T(\text{HJD}) = 2451451.4040(5) + 4.89380(3) \times E, \quad (1)$$

The stars are nearly spherical; the radius of the primary varies by 2% depending on the direction (towards the pole, inner Lagrangian point, side, back), while the variation in the secondary is less than 1%. We used the volume radius to compute the surface area of the stars for our distance calculation. The WD values yield masses $M_1 = 33.4 \pm 3.5 M_{\odot}$, $M_2 = 30.0 \pm 3.3 M_{\odot}$, radii $R_1 = 12.3 \pm 0.4 R_{\odot}$, $R_2 = 8.8 \pm 0.3 R_{\odot}$, and values for $\log(g)$ of 3.78 for the primary and 4.03 for the secondary. The flux ratio derived from the luminosity and radius ratio is $F_1/F_2 = 1.040$ in V -band and $F_1/F_2 = 1.047$ in B -band. This implies a temperature difference of 1000 K to 1500 K in the temperature range considered and at the gravities of the two objects.

We initially allowed the third light to be a free parameter, however, after converging to negative values, we set it to zero. The presence of deep eclipses additionally gives us confidence that there is no significant blending/crowding effect present. We fixed $d\omega/dt$ to zero since the residuals did not reveal any significant trend from the two year baseline of our photometry.

3.4. Determination of Effective Temperatures

The effective temperatures of the stars were determined by fitting the observed spectra with FASTWIND spectra. We adopted solar metallicity in the models appropriate for a deprojected galactocentric radius of $460''$ for the DEB, according to Zaritsky et al. (1989); Urbaneja et al. (2005). The value of $\log(g)$ and the flux ratio were both fixed to the values found from the analysis of the light and radial velocity curves (see §3.3). We used $v_{turb} = 0$ as appropriate (see Repolust et al. 2004) and $N(He)/N(H) = 0.1$, the measured $v \sin i$ of 120 km s^{-1} , and adopted values for the mass loss rates of $\dot{M} = 6.7 \cdot 10^{-7} M_{\odot} \text{ yr}^{-1}$ for the primary and $1.7 \cdot 10^{-7} M_{\odot} \text{ yr}^{-1}$ for the cooler secondary. This choice of mass-loss rates is justified by the fit of the mass-loss dependent HeII line $\lambda 4686$ (see Repolust et al. 2005; Massey et al. 2004, 2005), shown in Figure 8. It also agrees with the average values found by Repolust et al. (2005) for stars of similar parameters. The terminal velocities of the stellar wind are correlated with the photospheric escape velocities. Following Kudritzki & Puls (2000), we adopted for the former 2200 km/s and 2600 km/s .

We combined spectra near quadratures (phases 0.26 and 0.68) with similar radial velocities, degrading the ESI spectra to match GMOS resolution and dispersion where appropriate. The difference in the velocities is between $0 - 60 \text{ km s}^{-1}$, which corresponds to a maximum shift of 0.9 \AA in our wavelength range, and does not affect the temperature determination. We fit composite model spectra to all the helium lines in our wavelength range except HeI $\lambda 4713$, which was too noisy to use quantitatively. However, the fits were in agreement with this line as well. The composite spectra were calculated as follows:

$$F_{\lambda} = w_1 F_{1,\lambda}(T_1) + w_2 F_{2,\lambda}(T_2) \quad (2)$$

where

$$w_1 = \frac{1}{1 + (R_1/R_2)^2 F_2/F_1} \quad \text{and} \quad w_2 = 1 - w_1 \quad (3)$$

The ratio of the radii and fluxes were fixed to the values derived in the previous Section, therefore the only free parameter was T_1 . The HeII $\lambda 4542$ /HeI $\lambda 4471$ ratio measured from the spectra indicated a spectral type of O7 for both stars. In this regime, the helium line

strengths are quite sensitive to temperature. The HeII line equivalent widths increase with increasing effective temperature, whereas the HeI widths decrease. Figure 5 illustrates this dependence for several lines. Finally, we resolved the degeneracy in the radii from the information in the spectra by determining that the slightly hotter primary contributes twice as much light, thus forcing it to be the larger star.

The temperature of the primary was derived from a simultaneous fit to the following 7 lines: HeI $\lambda\lambda$ 4026, 4388, 4471, 4921 and HeII $\lambda\lambda$ 4200, 4542, 4686. Figures 6, 7 and 8 show fits to the helium lines at each quadrature. The fits to the Balmer lines shown in Figures 9 and 10 demonstrate that the model atmospheres reproduce the spectra correctly with the gravities derived from the light and radial velocity curve analysis. The strong emission lines in the center of the hydrogen and some of the helium lines originate in nearby H II regions. The effective temperature of the secondary follows from the flux ratio and is consistent with the spectral fit of the lines from the secondary as displayed in the Figures. We found the best fit temperature for all the helium lines to be $T_{\text{eff},1} = 37000 \pm 1500$ K, and consequently $T_{\text{eff},2} = 35600 \pm 1500$ K.

4. Distance Determination

The flux f_λ measured at Earth at a certain wavelength λ from a binary at distance d is given by

$$f_\lambda = \frac{1}{d^2} (R_1^2 F_{1,\lambda} + R_2^2 F_{2,\lambda}) \times 10^{-0.4 A(\lambda)}, \quad (4)$$

where R_1 and R_2 are the radii of the two stars and $F_{1,\lambda}$ and $F_{2,\lambda}$ the surface fluxes. The total extinction $A(\lambda)$ is a function of the reddening $E(B - V)$, the normalized extinction curve $k(\lambda - V) \equiv E(\lambda - V)/E(B - V)$ and the ratio of total to selective extinction in the V band $R \equiv A(V)/E(B - V)$:

$$A(\lambda) = E(B - V) [k(\lambda - V) + R]. \quad (5)$$

Having measured the temperatures of the stars from the spectra, we computed fluxes and fit to the observed magnitudes, using equation 4 and FASTWIND model atmospheres with $T_{\text{eff},1} = 37000$ K and $T_{\text{eff},2} = 35000$ K. We calculated synthetic photometry of the composite spectrum over the appropriate Johnson-Cousins optical filter functions as defined by Bessell (1990) and calibrated by Landolt (1992), and the 2MASS filter set. Monochromatic fluxes were measured at the isophotal wavelengths (see Tokunaga & Vacca 2005), which best

represent the flux in a passband. We used zeropoints from Bessell et al. (1998, Appendix A) and Cohen et al. (2003) to convert the fluxes to magnitudes. We reddened the model spectrum using the reddening law parameterization of Cardelli et al. (1989), as prescribed in Schlegel et al. (1998), and simultaneously fit the optical and near-infrared $BVRJHK_s$ photometry. Specifically, we computed the intrinsic $(B - V)_0 = -0.29$ from the model atmospheres at the isophotal wavelengths, thus yielding $E(B - V) = 0.09 \pm 0.01$. The best fit that minimized the photometric error over the 6 photometric bands was given by $R_V = 3.5 \pm 0.5$. The resulting distance modulus to the DEB and thus M33 is 24.92 ± 0.12 mag (964 ± 54 kpc). The fit of the reddened model spectrum to the photometry is shown in Figure 11 and the residuals in Figure 12. The U and I values from Massey et al. (2006) are shown but not used in the fit because there are inherent problems with U -band photometry (see discussion in Massey 2002) and the I -band often suffers from fringing effects. The BVR photometry alone, assuming $R_V = 3.1$ and $E(B - V) = 0.09$, yields a distance modulus of 24.95 mag, demonstrating the consistency of the near-infrared with the optical photometry.

The uncertainty in the distance was computed by adding in quadrature the individual conservative errors: 4% in the radii which translates to 0.085 mag in the distance modulus, 4% in $T_{\text{eff},1}$ which corresponds to 0.06 mag, 0.04 mag from the SED fit, assuming $R_V = 3.5 \pm 0.5$ and $E(B - V) = 0.09 \pm 0.01$, and 0.03 mag in the flux. The error in the flux results from adding in quadrature the statistical 0.01 mag uncertainty from the fit to $BVRJHK_s$ and the 0.03 mag uncertainty in the zeropoints. The total uncertainty is thus 0.12 mag. We did not attempt a full statistical treatment, since the error is dominated by the uncertainty in the radii. Note, that at these high temperatures the $B - V$ color of stars saturates, giving a weak dependence of the distance modulus on T_{eff} .

As an independent check on our reddening and extinction determination we used Chrizos (Maíz-Apellániz 2004). We first generated a grid of TLUSTY models (Lanz & Hubeny 2003) at solar metallicity in the temperature and gravity regime of interest and fixed the effective temperature to 37000 K and $\log(g) = 3.80$. The χ^2 minimization fit to the $BVJHK_s$ photometry resulted in $R_{5495} = 3.7 \pm 0.5$ and $E(4405 - 5495) = 0.07 \pm 0.01$, in agreement with the FASTWIND analysis. Note, that we computed these values at the isophotal wavelengths, which are bluer. We adopted these errors in the error analysis above.

5. Discussion

We present the first distance to a detached eclipsing binary in M33, establishing it as an independent rung on the cosmological distance ladder. This distance determination is a significant step towards replacing the current anchor galaxy of the extragalactic distance

scale, the LMC, with galaxies more similar to those in the HST Key Project (Freedman et al. 2001), such as M33 and M31. We have chosen a detached eclipsing binary to simplify the modeling and derived a distance modulus of 24.92 ± 0.12 mag.

D33J013346.2+304439.9 is located in the rich OB 66 association (Humphreys & Sandage 1980), which contains a relatively high massive star population (Massey et al. 1995). The presence of one of the best candidate detached eclipsing binaries for distance determination in this association is not surprising. In addition to the DEB, OB 66 contains several other eclipsing binaries (see Paper VI), which suggests a high binary star formation rate for massive stars. Our adopted color excess value $E(B - V) = 0.09 \pm 0.01$ is smaller than estimations from Massey et al. (1995) for OB 66. Using the “ q method” and UBV photometry of 36 stars, they derive $E(B - V) = 0.15 \pm 0.02$ and their spectroscopic sample yields $E(B - V) = 0.13 \pm 0.01$. However, our multi-band photometry combined with the spectroscopy determines the reddening accurately, thus it is unlikely our distance estimation suffers from systematic errors due to reddening.

There are several avenues for improving the distance to M33 and M31 using eclipsing binaries. Wyithe & Wilson (2002) propose the use of semi-detached eclipsing binaries to be just as good or better distance indicators as detached eclipsing binaries, which have been traditionally considered to be ideal. The use of new improved stellar atmosphere models to derive surface brightnesses versus calibrations based on interferometry removes the restriction to DEBs for distance determination. Additionally, Wyithe & Wilson (2002) outline other benefits for using semi-detached binaries: their orbits are tidally circularized and their Roche lobe filling configurations provide an extra constraint in the parameter space, especially for complete eclipses ($i \sim 90$ deg). Bright semi-detached binaries in M33 or M31 are not as rare as DEBs, and are easier to follow-up spectroscopically, as demonstrated by Ribas et al. (2005) in M31. Thus, for the determination of the distances to M33 and M31 to better than 5% we suggest both determining distances to other bright DEBs and to semi-detached systems found by DIRECT and other variability surveys. Additional spectroscopy of the DEB would also improve the current distance determination to M33, since the errors are dominated by the uncertainty in the radius or velocity semi-amplitude.

How does our M33 distance compare to previous determinations? Table 7 presents a compilation of 13 recent distance determinations to M33 ranging from 24.32 to 24.92 mag, including the reddening values used. Our measurement although completely independent yields the largest distance with a small 6% error, thus is not consistent with some of the previous determinations. This possibly indicates unaccounted sources of systematic error in the calibration of certain distance indicators.

The implications of our result on the extragalactic distance scale are significant, espe-

cially when comparing to the *HST* Key Project (Freedman et al. 2001) distance to M33. They derive a metallicity corrected Cepheid distance of 24.62 ± 0.15 mag, using a high reddening value of $E(V - I) = 0.27$ and an assumed LMC distance modulus of 18.50 ± 0.10 mag. If we calculate the LMC distance our result would imply, we derive 18.80 ± 0.16 mag, which is not consistent with the eclipsing binary determinations. The error is obtained by adding in quadrature the individual errors in the two distance measurements. Taking this one step further, our LMC distance would imply a 15% decrease in the Hubble constant to $H_0 = 61 \text{ km s}^{-1} \text{ Mpc}^{-1}$. This improbable result brings into question the Key Project metallicity corrections and reddening values not only for M33, but also for the other galaxies in the Key Project. We thus demonstrate the importance of accurately calibrating the distance scale and determining H_0 , which are both vital for constraining the dark energy equation of state (Hu 2005) and complementing the cosmic microwave background measurements from the Wilkinson Microwave Anisotropy Probe (WMAP; Spergel et al. 2006).

We are very grateful to Bohdan Paczyński for motivating us to undertake this project almost a decade ago. We thank Phil Massey for sending us his photometry of the DEB from his Local Group Survey before publication. We would like to thank the staff of the Mt. Hopkins observatory for their support during extensive observing campaigns and the anonymous referee for comments that improved the manuscript. AZB and KZS were partially supported by HST Grant HST-GO-09810.06-A. AZB acknowledges research and travel support from the Carnegie Institution of Washington through a Vera Rubin Fellowship. Support for L.M.M. was provided by NASA through Hubble Fellowship grant HST-HF-01153 from the Space Telescope Science Institute and by the National Science Foundation through a Goldberg Fellowship from the National Optical Astronomy Observatory. JK was supported by MNI grant 1P03D001-28. BJM was supported by the Polish KBN grant 1P03D01230. GT acknowledges partial support from NSF grant AST-0406183.

Some of the data presented herein were obtained at the W.M. Keck Observatory, which is operated as a scientific partnership among the California Institute of Technology, the University of California and the National Aeronautics and Space Administration. The Observatory was made possible by the generous financial support of the W.M. Keck Foundation. The authors wish to recognize and acknowledge the very significant cultural role and reverence that the summit of Mauna Kea has always had within the indigenous Hawaiian community. We are most fortunate to have the opportunity to conduct observations from this mountain. This paper is also based on observations obtained under Program ID GN-2004B-Q-25 and GN-2005B-DD-4 at the Gemini Observatory, which is operated by the Association of Universities for Research in Astronomy, Inc., under a cooperative agreement with the NSF on behalf of the Gemini partnership: the National Science Foundation (United States), the

Particle Physics and Astronomy Research Council (United Kingdom), the National Research Council (Canada), CONICYT (Chile), the Australian Research Council (Australia), CNPq (Brazil) and CONICET (Argentina). This publication makes use of data products from the Two Micron All Sky Survey, which is a joint project of the University of Massachusetts and the Infrared Processing and Analysis Center/California Institute of Technology, funded by the National Aeronautics and Space Administration and the National Science Foundation.

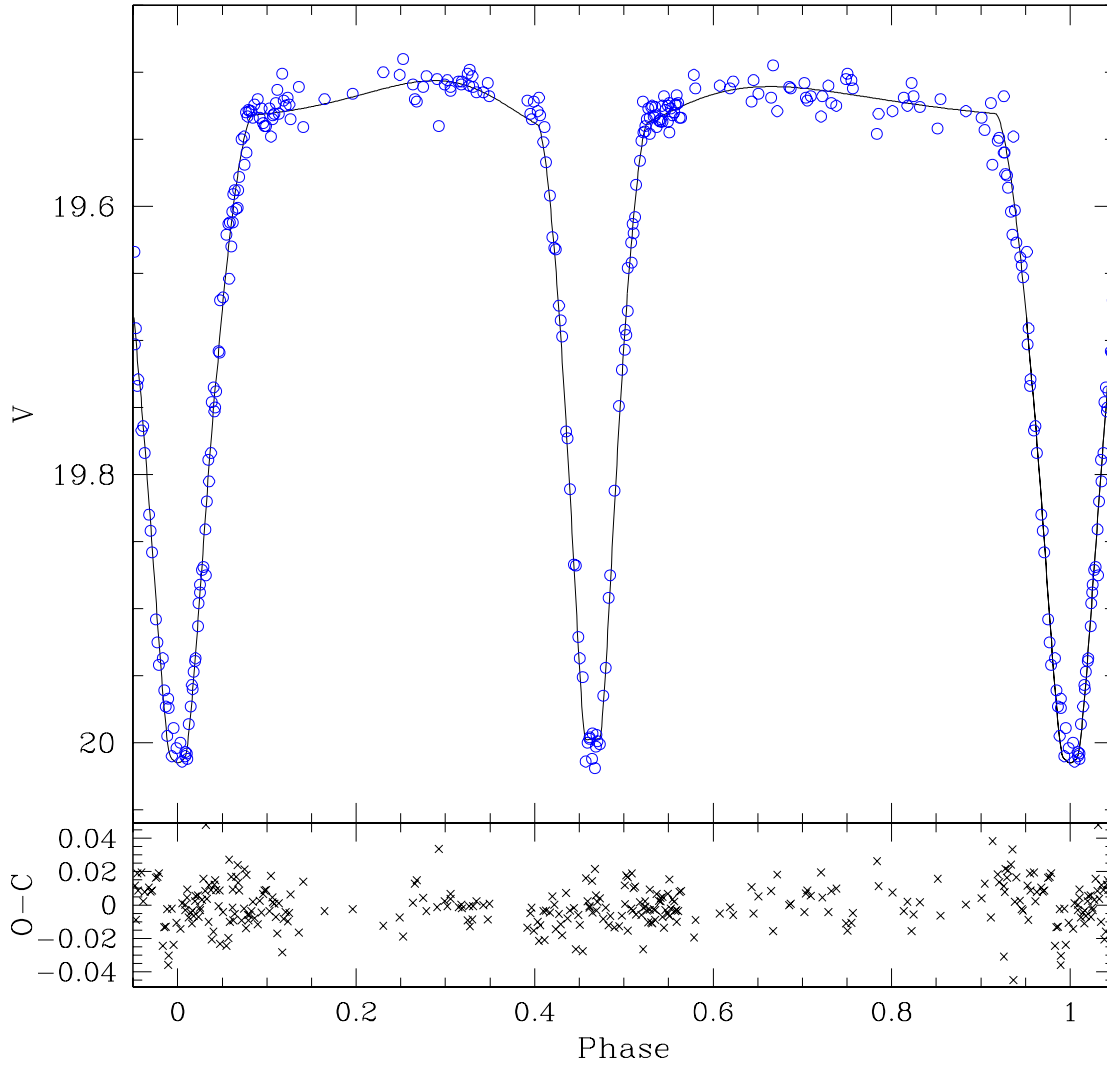


Fig. 2.— V -band light curve of the DEB with model fit from the Wilson-Devinney program. The rms is 0.01 mag.

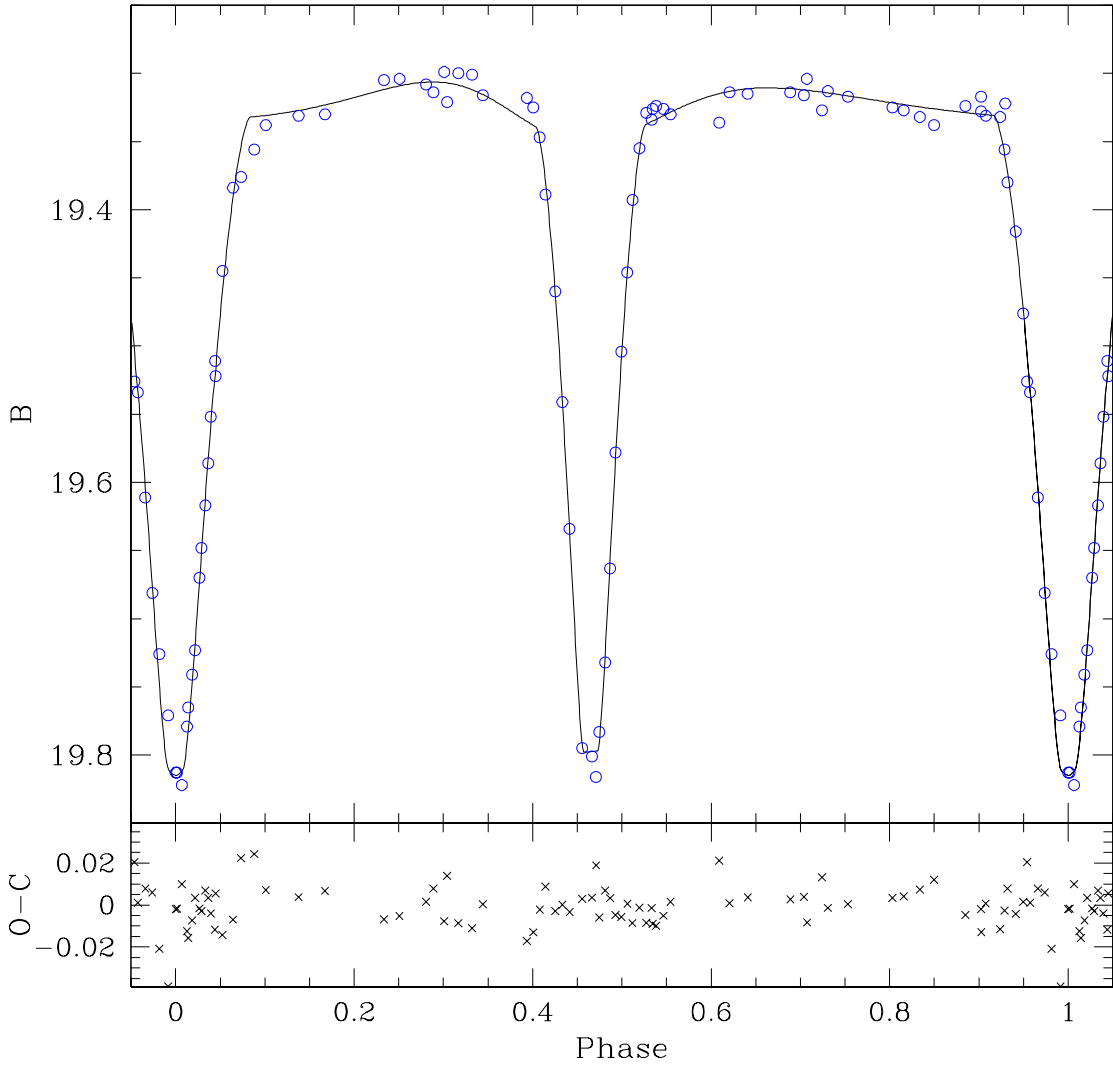


Fig. 3.— B -band light curve of the DEB with model fit from the Wilson-Devinney program. The rms is 0.01 mag.

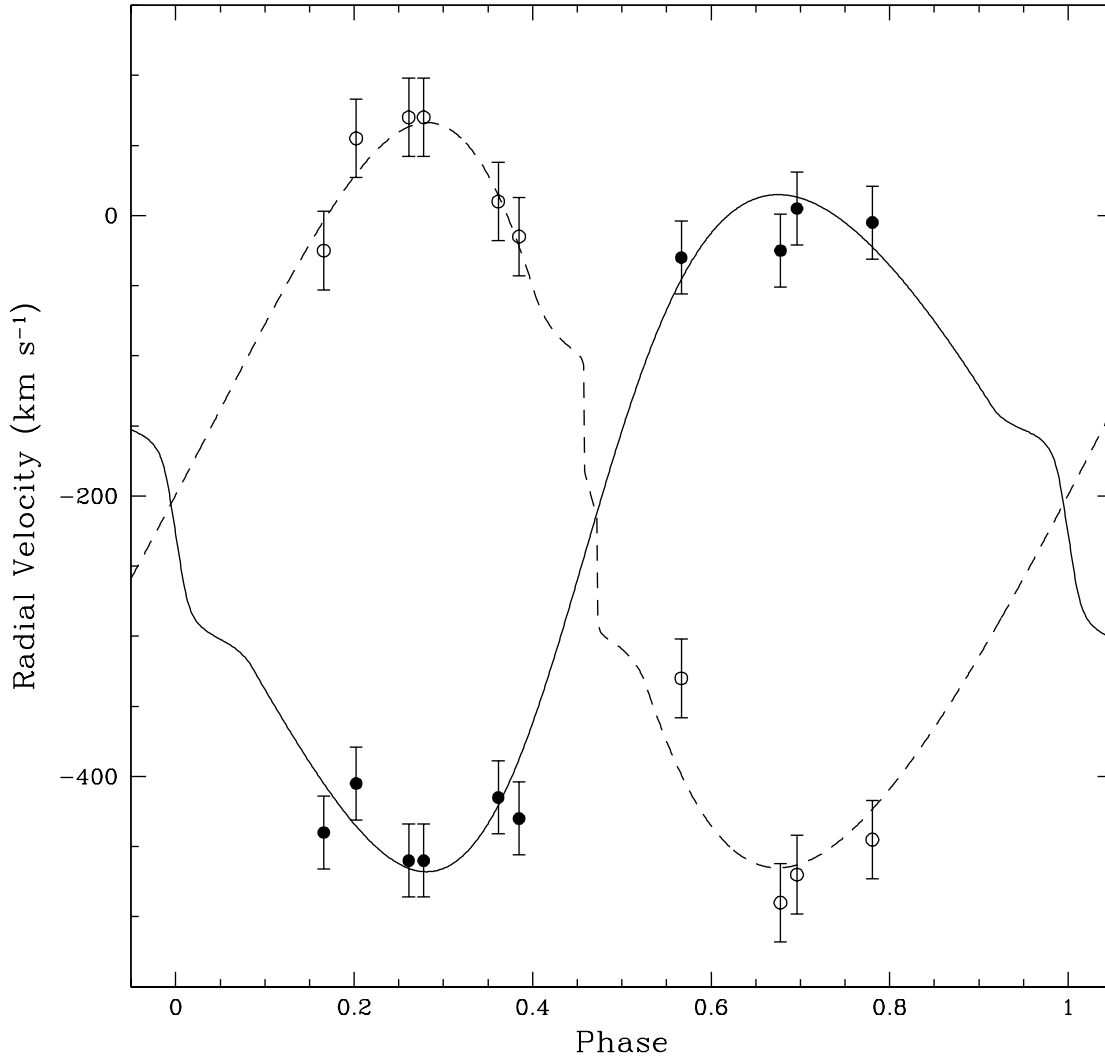


Fig. 4.— Radial velocities for the DEB measured by TODCOR with FASTWIND synthetic spectra. Model fit is from Wilson-Devinney program, including the Rossiter effect. Error bars correspond to the rms of the fit: 26.0 km s⁻¹ for the primary (filled circles) and 28.0 km s⁻¹ for the secondary (open circles).

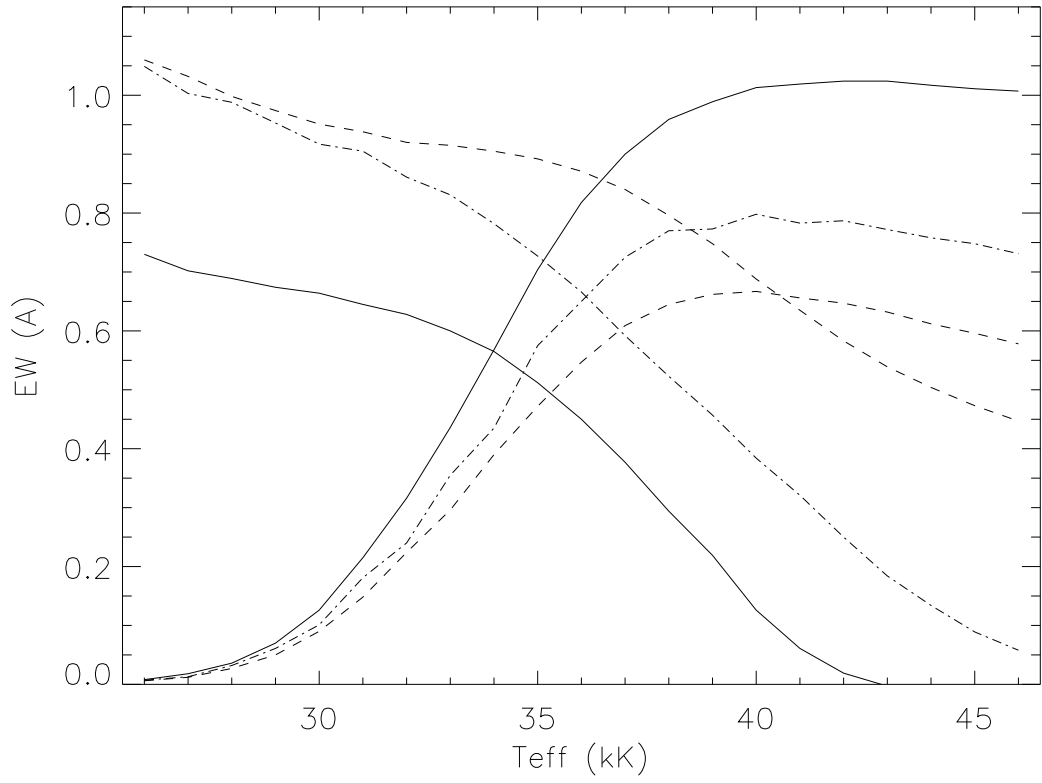


Fig. 5.— Equivalent widths of helium lines vs. T_{eff} . The HeI line strengths decrease with increasing T_{eff} (solid: $\lambda 4921$, dashed-dotted: $\lambda 4471$, dashed: $\lambda 4026$); the HeII line strengths increase (solid: $\lambda 5411$, dashed-dotted: $\lambda 4542$, dashed: $\lambda 4200$).

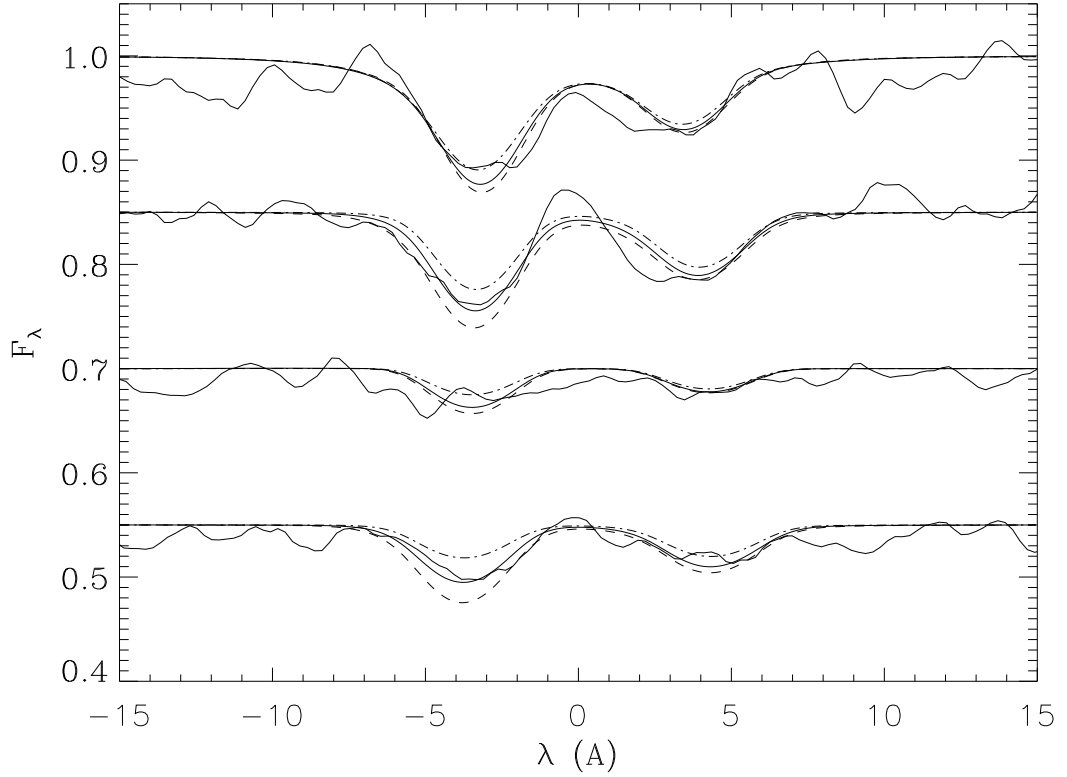


Fig. 6.— Fit of the composite spectra of HeI lines at phase 0.26. At this phase the absorption lines originating in the primary are blue-shifted, whereas the lines from the secondary are red-shifted. Rectified spectra corrected for the gamma velocity are plotted as a function of wavelength displacement from the atomic line transition wavelength. The lines from top to bottom are HeI $\lambda\lambda$ 4026, 4471, 4713, 4921 and have been shifted in flux by 0.15 for clarity. Overplotted are the model calculations as described in the text. The solid curve represents our final model corresponding to a primary effective temperature of 37000K. The dashed and the dashed-dotted curves represent primary temperatures of 39000K and 35000K, respectively.

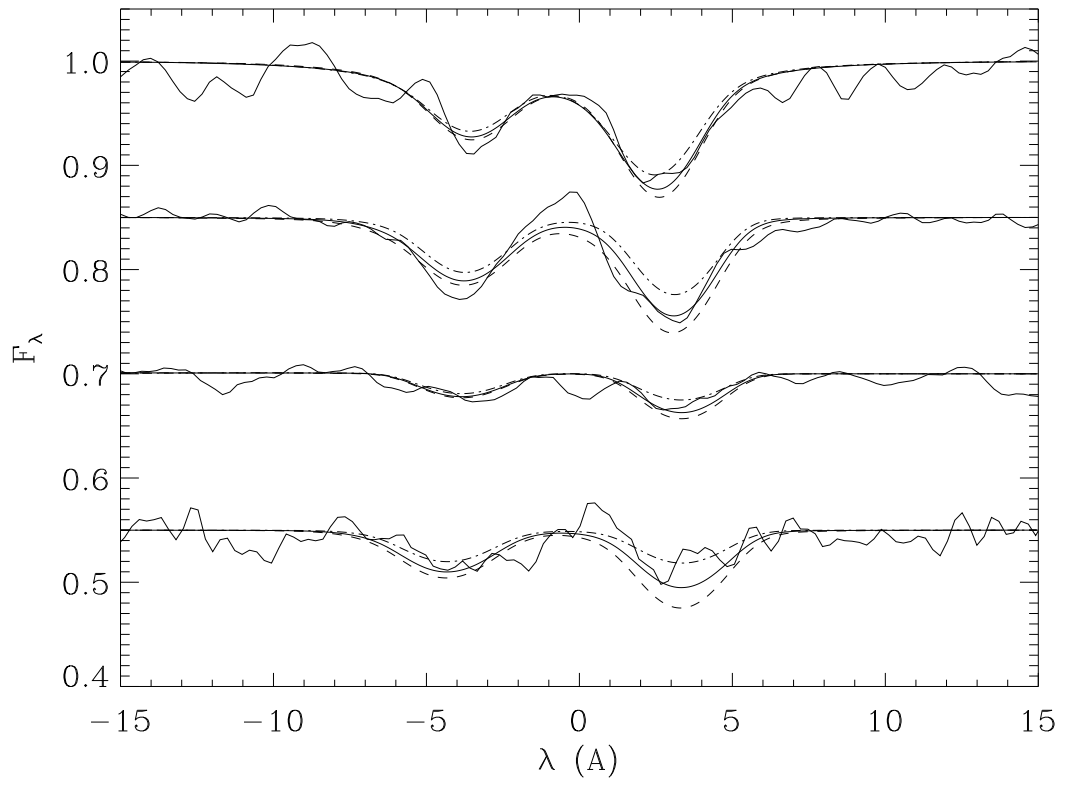


Fig. 7.— Same as Figure 6, but at phase 0.68, where the lines from the primary (secondary) are red-shifted (blue-shifted).

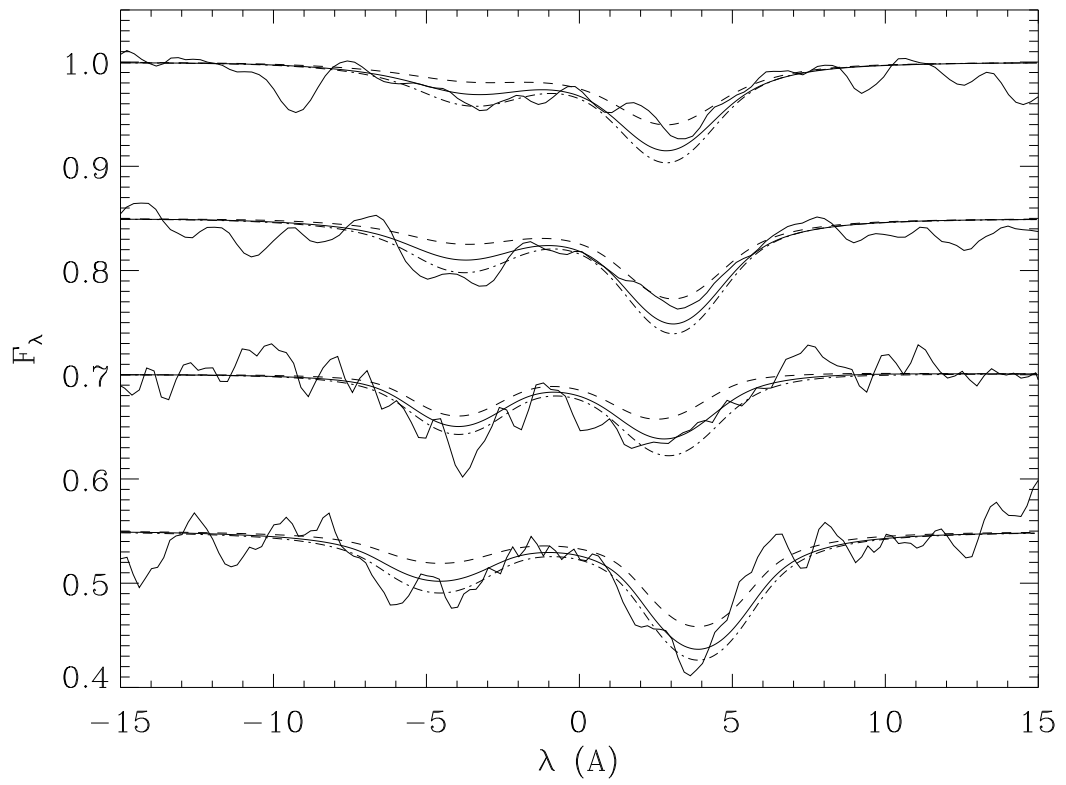


Fig. 8.— Same as Figure 7, but for the HeII lines. Plotted are HeII $\lambda\lambda 4200$, 4542 , 4686 , 5411 from top to bottom.

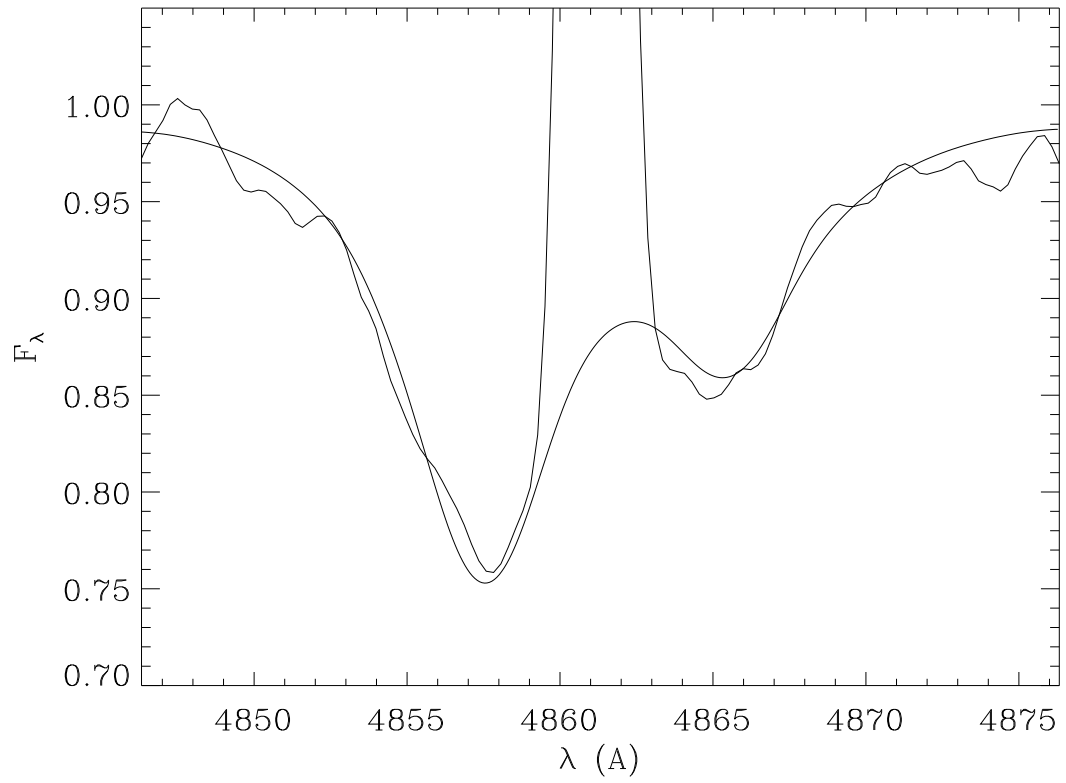


Fig. 9.— Plot of the $H\beta$ profile at phase 0.26 compared to the final model.

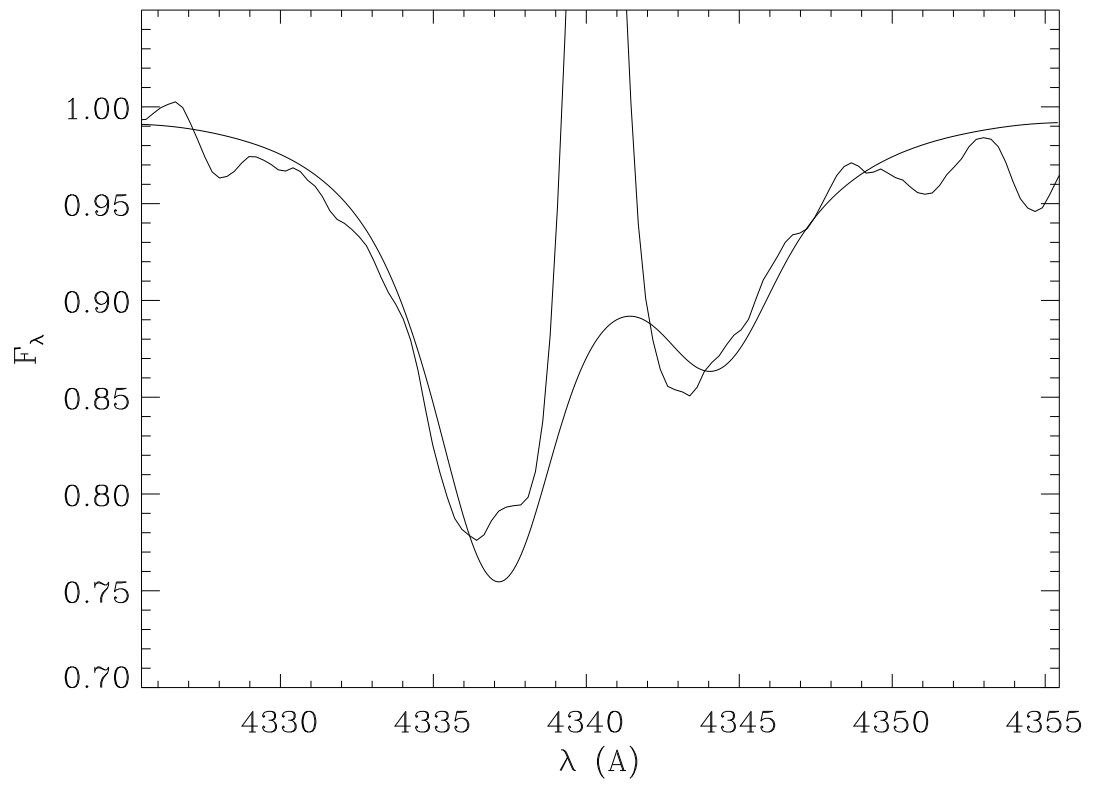


Fig. 10.— Same as Figure 9, but for $H\gamma$.

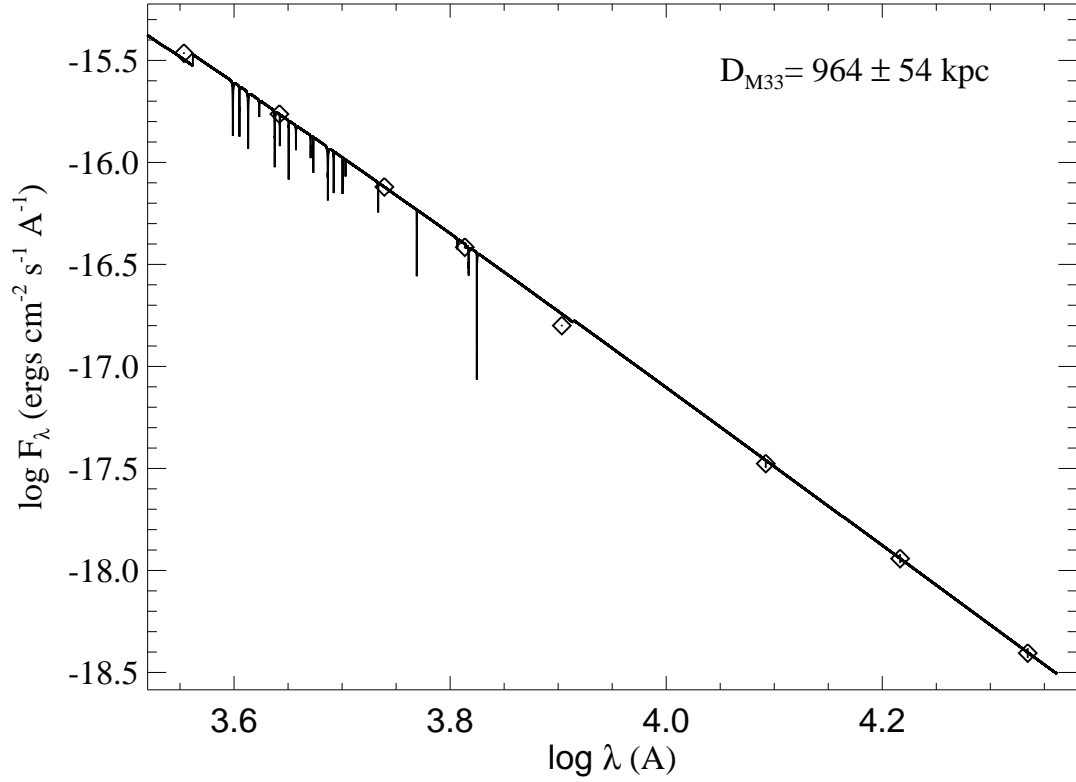


Fig. 11.— Fit of the reddened DEB model spectrum to the $BVRJHK_s$ ground-based photometry. Overplotted is the U and I photometry from Massey et al. (2006). The best fit values of $E(B - V) = 0.09 \pm 0.01$ and $R_V = 3.5 \pm 0.5$ yield a distance modulus to the DEB and thus M33 of 24.92 ± 0.12 mag (964 ± 54 kpc).

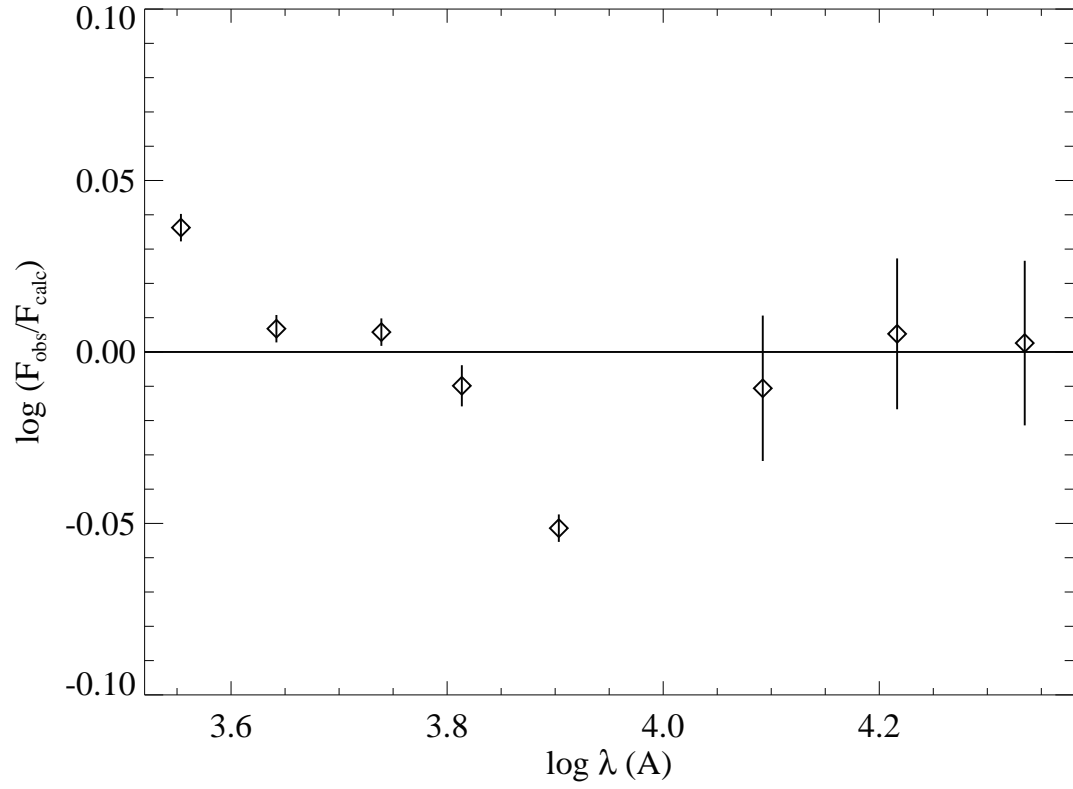


Fig. 12.— Residuals of the SED fit, in terms of the flux ratio. The error in the fit to the $BVRJHK_s$ photometry corresponds to 0.01 mag. U and I are shown, but not used in the fit. Error bars correspond to the photometric error for each band in flux units.

REFERENCES

- Alard, C. 2000, *A&AS*, 144, 363
- Alard, C. & Lupton, R. H. 1998, *ApJ*, 503, 325
- Andersen, J. 1991, *A&A Rev.*, 3, 91
- Benedict, G. F., McArthur, B. E., Fredrick, L. W., et al. 2002, *AJ*, 123, 473
- Bessell, M. S. 1990, *PASP*, 102, 1181
- Bessell, M. S., Castelli, F., & Plez, B. 1998, *A&A*, 333, 231
- Bonanos, A. Z., Stanek, K. Z., Sasselov, D. D., et al. 2003, *AJ*, 126, 175
- Brunthaler, A., Reid, M. J., Falcke, H., et al. 2005, *Science*, 307, 1440
- Cardelli, J. A., Clayton, G. C., & Mathis, J. S. 1989, *ApJ*, 345, 245
- Ciardullo, R., Durrell, P. R., Laychak, M. B., et al. 2004, *ApJ*, 614, 167
- Claret, A. 2000, *A&A*, 363, 1081
- Cohen, M., Wheaton, W. A., & Megeath, S. T. 2003, *AJ*, 126, 1090
- Fitzpatrick, E. L., Ribas, I., Guinan, E. F., et al. 2003, *ApJ*, 587, 685
- Freedman, W. L., Madore, B. F., Gibson, B. K., et al. 2001, *ApJ*, 553, 47
- Galleti, S., Bellazzini, M., & Ferraro, F. R. 2004, *A&A*, 423, 925
- Guinan, E. F., Fitzpatrick, E. L., Dewarf, L. E., et al. 1998, *ApJ*, 509, L21
- Harmanec, P., Hadrava, P., Yang, S., et al. 1997, *A&A*, 319, 867
- Harries, T. J., Hilditch, R. W., & Howarth, I. D. 2003, *MNRAS*, 339, 157
- Hilditch, R. W. 1996, in *ASP Conf. Ser. 90: The Origins, Evolution, and Destinies of Binary Stars in Clusters*, ed. E. F. Milone & J.-C. Mermilliod (San Francisco: ASP), 207
- Hilditch, R. W. 2001, *An Introduction to Close Binary Stars (An Introduction to Close Binary Stars, by R.W. Hilditch. Cambridge University Press, 2001, 392 pp.)*
- Hilditch, R. W., Howarth, I. D., & Harries, T. J. 2005, *MNRAS*, 357, 304
- Hodapp, K. W., Jensen, J. B., Irwin, E. M., et al. 2003, *PASP*, 115, 1388

- Hook, I., Allington-Smith, J. R., Beard, S. M., et al. 2003, in *Instrument Design and Performance for Optical/Infrared Ground-based Telescopes*. Edited by Iye, Masanori; Moorwood, Alan F. M. *Proceedings of the SPIE*, Volume 4841, pp. 1645-1656 (2003)., 1645–1656
- Hu, W. 2005, in *ASP Conf. Ser. 339: Observing Dark Energy*, 215–+
- Humphreys, R. M. & Sandage, A. 1980, *ApJS*, 44, 319
- Ilijic, S., Hensberge, H., & Pavlovski, K. 2001, *Fizika B*, 10, 357
- Ilijic, S., Hensberge, H., Pavlovski, K., et al. 2004, in *ASP Conf. Ser. 318: Spectroscopically and Spatially Resolving the Components of the Close Binary Stars*, 111–113
- Ivanov, G. R., Freedman, W. L., & Madore, B. F. 1993, *ApJS*, 89, 85
- Kallrath, J. & Milone, E. F., eds. 1999, *Eclipsing binary stars : modeling and analysis*
- Kaluzny, J., Mochejska, B. J., Stanek, K. Z., et al. 1999, *AJ*, 118, 346
- Kaluzny, J., Stanek, K. Z., Krockenberger, M., et al. 1998, *AJ*, 115, 1016
- Kim, M., Kim, E., Lee, M. G., et al. 2002, *AJ*, 123, 244
- Kruszewski, A. & Semeniuk, I. 1999, *Acta Astronomica*, 49, 561
- Kudritzki, R. & Puls, J. 2000, *ARA&A*, 38, 613
- Kurtz, M. J., Mink, D. J., Wyatt, W. F., et al. 1992, in *ASP Conf. Ser. 25: Astronomical Data Analysis Software and Systems I*, 432–+
- Kurucz, R. 1993, *ATLAS9 Stellar Atmosphere Programs and 2 km/s grid*. Kurucz CD-ROM No. 13. Cambridge, Mass.: Smithsonian Astrophysical Observatory, 1993., 13
- Landolt, A. U. 1992, *AJ*, 104, 340
- Lanz, T. & Hubeny, I. 2003, *ApJS*, 146, 417
- Lee, M. G., Kim, M., Sarajedini, A., et al. 2002, *ApJ*, 565, 959
- Macri, L. M., Stanek, K. Z., Sasselov, D. D., et al. 2001, *AJ*, 121, 870
- Maíz-Apellániz, J. 2004, *PASP*, 116, 859
- Massey, P. 2002, *ApJS*, 141, 81

- Massey, P., Armandroff, T. E., Pyke, R., et al. 1995, *AJ*, 110, 2715
- Massey, P., Bianchi, L., Hutchings, J. B., & Stecher, T. P. 1996, *ApJ*, 469, 629
- Massey, P., Bresolin, F., Kudritzki, R. P., et al. 2004, *ApJ*, 608, 1001
- Massey, P., Olsen, K. A. G., Hodge, P. W., et al. 2006, *AJ*, 131, 2478
- Massey, P., Puls, J., Pauldrach, A. W. A., et al. 2005, *ApJ*, 627, 477
- Matheson, T., Filippenko, A. V., Ho, L. C., et al. 2000, *AJ*, 120, 1499
- McConnachie, A. W., Irwin, M. J., Ferguson, A. M. N., et al. 2004, *MNRAS*, 350, 243
- Mochejska, B. J., Kaluzny, J., Stanek, K. Z., et al. 1999, *AJ*, 118, 2211
- . 2001a, *AJ*, 121, 2032
- . 2001b, *AJ*, 122, 2477
- Mochejska, B. J., Macri, L. M., Sasselov, D. D., et al. 2000, *AJ*, 120, 810
- . 2001c, *astro-ph/0103440*
- Nelson, B. & Davis, W. D. 1972, *ApJ*, 174, 617
- Paczynski, B. 1997, in *The Extragalactic Distance Scale*, 273–280
- Pierce, M. J., Jurcevic, J. S., & Crabtree, D. 2000, *MNRAS*, 313, 271
- Popper, D. M. & Etzel, P. B. 1981, *AJ*, 86, 102
- Press, W. H., Teukolsky, S. A., Vetterling, W. T., et al. 1992, *Numerical recipes in FORTRAN. The art of scientific computing* (Cambridge: University Press, —c1992, 2nd ed.)
- Puls, J., Urbaneja, M. A., Venero, R., et al. 2005, *A&A*, 435, 669
- Pych, W. 2004, *PASP*, 116, 148
- Repolust, T., Puls, J., Hanson, M. M., et al. 2005, *A&A*, 440, 261
- Repolust, T., Puls, J., & Herrero, A. 2004, *A&A*, 415, 349
- Ribas, I., Jordi, C., Vilardell, F., et al. 2005, *ApJ*, 635, L37
- Santolaya-Rey, A. E., Puls, J., & Herrero, A. 1997, *A&A*, 323, 488

- Sarajedini, A., Barker, M., Geisler, D., et al. 2006, AJ, in press (astro-ph/0605580)
- Sarajedini, A., Geisler, D., Schommer, R., et al. 2000, AJ, 120, 2437
- Schlegel, D. J., Finkbeiner, D. P., & Davis, M. 1998, ApJ, 500, 525
- Schwarzenberg-Czerny, A. 1989, MNRAS, 241, 153
- . 1996, ApJ, 460, L107+
- Sheinis, A. I., Bolte, M., Epps, H., et al. 2002, PASP, 114, 851
- Simon, K. P. & Sturm, E. 1994, A&A, 281, 286
- Spergel, D. N., Bean, R., Dore, O., et al. 2006, ApJ, submitted (astro-ph/0603449)
- Stanek, K. Z., Kaluzny, J., Krockenberger, M., et al. 1998, AJ, 115, 1894
- . 1999, AJ, 117, 2810
- Stetson, P. B. 1987, PASP, 99, 191
- . 1990, PASP, 102, 932
- Tiede, G. P., Sarajedini, A., & Barker, M. K. 2004, AJ, 128, 224
- Tokunaga, A. T. & Vacca, W. D. 2005, PASP, 117, 421
- Tonry, J. & Davis, M. 1979, AJ, 84, 1511
- Urbaneja, M.-A., Herrero, A., Kudritzki, R.-P., et al. 2005, ApJ, 635, 311
- van Hamme, W. 1993, AJ, 106, 2096
- van Hamme, W. & Wilson, R. E. 2003, in ASP Conf. Ser. 298: GAIA Spectroscopy: Science and Technology, 323
- Wade, R. A. & Horne, K. 1988, ApJ, 324, 411
- Wilson, R. E. 1979, ApJ, 234, 1054
- . 1990, ApJ, 356, 613
- Wilson, R. E. & Devinney, E. J. 1971, ApJ, 166, 605
- Wyithe, J. S. B. & Wilson, R. E. 2002, ApJ, 571, 293

Zaritsky, D., Elston, R., & Hill, J. M. 1989, AJ, 97, 97

Zucker, S. & Mazeh, T. 1994, ApJ, 420, 806

Table 1. *V*–BAND DEB LIGHT CURVE

HJD ^a	<i>V</i>	σ_{mag}
1451.6862	19.654	0.007
1451.6979	19.630	0.008
1451.7073	19.612	0.008
1451.7241	19.602	0.008
1451.7329	19.601	0.008

^aHJD-2450000

Note. — Table 1 is available in its entirety in the electronic version of the Journal. A portion is shown here for guidance regarding its form and content.

Table 2. *B*–BAND DEB LIGHT CURVE

HJD ^a	<i>B</i>	σ_{mag}
1451.7623	19.376	0.010
1451.8347	19.356	0.009
1451.8981	19.338	0.007
1452.8169	19.314	0.008
1452.8922	19.321	0.008

^aHJD-2450000

Note. — Table 2 is available in its entirety in the electronic version of the Journal. A portion is shown here for guidance regarding its form and content.

Table 3. SPECTROSCOPIC OBSERVATIONS

UT Obs. Date	Telescope	Instr.	# exp.	Total exp. time (hours)	Mid. Exp. HJD
20021031	Keck-2	ESI	4	1.53	2452578.8611
20021101	Keck-2	ESI	2	0.575	2452579.8873
20030903	Keck-2	ESI	5	2.92	2452886.0960
20030904	Keck-2	ESI	4	3.25	2452887.0532
20030905	Keck-2	ESI	4	3.20	2452888.0598
20040816	Gemini	GMOS-N	5	3.75	2453234.0229
20040818	Gemini	GMOS-N	5	3.75	2453236.0637
20040912	Gemini	GMOS-N	5	3.75	2453261.0327
20041009	Gemini	GMOS-N	5	3.75	2453287.9396
20041011	Keck-2	ESI	7	5.25	2453289.9871
20041112	Keck-2	ESI	3	4.50	2453321.8224

Table 4. HELIOCENTRIC RADIAL VELOCITY MEASUREMENTS FOR THE DEB

Mid. Exp. HJD	Orbital Phase	RV_1 ($km\ s^{-1}$)	RV_2 ($km\ s^{-1}$)	$(O - C)_1$ ($km\ s^{-1}$)	$(O - C)_2$ ($km\ s^{-1}$)
2452578.8611	0.386	-430	-15	-42	7
2452579.8873	0.595	-20	-560	-8	-124
2452886.0960	0.167	-440	-30	-35	-21
2452887.0532	0.362	-415	10	6	-4
2452888.0598	0.568	-35	-320	16	69
2453234.0229	0.260	-460	70	5	7
2453236.0637	0.677	-25	-490	-40	-25
2453261.0327	0.779	-5	-445	17	-22
2453287.9396	0.278	-460	70	8	4
2453289.9871	0.698	5	-475	-8	-7
2453321.8224	0.203	-410	55	30	25

Table 5. RESULTS FROM COMBINED *LC* AND *RV* CURVE ANALYSIS WITH WILSON-DEVINNEY PROGRAM

Parameter	Value
Period, P	4.89380 ± 0.00003 days
Time of primary eclipse, HJD_0	$2451451.4040(5)$
Inclination, i	87.2 ± 0.5 deg
Eccentricity, e	0.18 ± 0.02
Longitude of periastron, ω	252.4 ± 1.0 deg
Surface potential, Ω_1	5.09 ± 0.03
Surface potential, Ω_2	6.29 ± 0.06
Light ratio in V , L_2/L_1	0.492 ± 0.005
Light ratio in B , L_2/L_1	0.493 ± 0.005
Mass ratio, q	0.91 ± 0.07
Systemic velocity, γ	-214 ± 7 km s $^{-1}$
Semi-major axis, a	48.4 ± 1.6 R $_{\odot}$
Semi-amplitude, K_1	242 ± 11 km s $^{-1}$
Semi-amplitude, K_2	266 ± 11 km s $^{-1}$
Radius, $r_{1,pole}$	0.248 ± 0.002
..... $r_{1,point}$	0.267 ± 0.002
..... $r_{1,side}$	0.252 ± 0.002
..... $r_{1,back}$	0.261 ± 0.002
..... r_1^*	0.254 ± 0.002
Radius, $r_{2,pole}$	0.180 ± 0.002
..... $r_{2,point}$	0.185 ± 0.002
..... $r_{2,side}$	0.181 ± 0.002
..... $r_{2,back}$	0.184 ± 0.002
..... r_2^*	0.182 ± 0.002

*Volume radius.

Table 6. DEB PHYSICAL PARAMETERS

Parameter	Primary	Secondary
Mass (M $_{\odot}$)	33.4 ± 3.5	30.0 ± 3.3
Radius (R $_{\odot}$)	12.3 ± 0.4	8.8 ± 0.3
$\log g$ (cgs)	3.78 ± 0.03	4.03 ± 0.03
T $_{eff}$ (K)	37000 ± 1500	35600 ± 1500
$\log L/L_{\odot}$	5.41 ± 0.17	5.05 ± 0.18

Table 7. RECENT DISTANCE DETERMINATIONS TO M33

Study	Method ^a	Distance Modulus	Reddening
This Work	DEB	24.92 ± 0.12	$E(B - V) = 0.09 \pm 0.01$
Sarajedini et al. (2006)	RR Lyrae	24.67 ± 0.08	$\sigma_{E(V-I)} = 0.30$
Brunthaler et al. (2005)	Water Masers	24.32 ± 0.45	—
Ciardullo et al. (2004)	PNe	$24.86^{+0.07}_{-0.11}$	$E(B - V) = 0.04$
Galleti et al. (2004)	TRGB	24.64 ± 0.15	$E(B - V) = 0.04$
McConnachie et al. (2004)	TRGB	24.50 ± 0.06	$E(B - V) = 0.042$
Tiede et al. (2004)	TRGB	24.69 ± 0.07	$E(B - V) = 0.06 \pm 0.02$
Kim et al. (2002)	TRGB	$24.81 \pm 0.04(r)^{+0.15}_{-0.11}(s)$	$E(B - V) = 0.04$
Kim et al. (2002)	RC	$24.80 \pm 0.04(r) \pm 0.05(s)$	$E(B - V) = 0.04$
Lee et al. (2002)	Cepheids	$24.52 \pm 0.14(r) \pm 0.13(s)$	$E(B - V) = 0.20 \pm 0.04$
Freedman et al. (2001)	Cepheids	24.62 ± 0.15	$E(V - I) = 0.27$
Pierce et al. (2000)	LPVs	24.85 ± 0.13	$E(B - V) = 0.10$
Sarajedini et al. (2000)	HB	24.84 ± 0.16	$\langle E(V - I) \rangle = 0.06 \pm 0.02$

^aDEB: detached eclipsing binary; TRGB: tip of the red giant branch; PNe: planetary nebulae; RC: the red clump; LPVs: long period variables; HB: horizontal branch stars.